Phasic, suprathreshold excitation and sustained inhibition underlie neuronal selectivity for short-duration sounds

Rishi K. Alluri[a], Gary J. Rose[a,1], Jessica L. Hanson[a], Christopher J. Leary[b], Gustavo A. Vasquez-Opazo[a], Jalina A. Graham[c], and Jeremy Wilkerson[d]

[a]Department of Biology, University of Utah, Salt Lake City, UT 84112; [b]Department of Biology, University of Mississippi, Oxford, MS 38677; [c]Neuroscience Program, University of California, Davis, CA 95616; and [d]TalkingApe.org, Redwood City, CA 94063

Edited by Eric I. Knudsen, Stanford University School of Medicine, Stanford, CA, and approved January 29, 2016 (received for review October 23, 2015)

Sound duration is important in acoustic communication, including speech recognition in humans. Although duration-selective auditory neurons have been found, the underlying mechanisms are unclear. To investigate these mechanisms we combined in vivo whole-cell patch recordings from midbrain neurons, extraction of excitatory and inhibitory conductances, and focal pharmacological manipulations. We show that selectivity for short-duration stimuli results from integration of short-latency, sustained inhibition with delayed, phasic excitation; active membrane properties appeared to amplify responses to effective stimuli. Blocking $GABA_A$ receptors attenuated stimulus-related inhibition, revealed suprathreshold excitation at all stimulus durations, and decreased short-pass selectivity without changing resting potentials. Blocking AMPA and NMDA receptors to attenuate excitation confirmed that inhibition tracks stimulus duration and revealed no evidence of postinhibitory rebound depolarization inherent to coincidence models of duration selectivity. These results strongly support an anticoincidence mechanism of short-pass selectivity, wherein inhibition and suprathreshold excitation show greatest temporal overlap for long duration stimuli.

whole-cell | GABA | synaptic conductance | gabazine | inferior colliculus

A principal goal in neuroscience is to understand the computational mechanisms that underlie selectivity for particular types of information. Sensory neurons have been identified that show selectivity for biologically relevant stimulus features; however, the underlying mechanisms are, in most cases, poorly understood. A notable exception involves mechanisms of selectivity for sound duration, particularly in bat and anuran auditory systems (1–3). Duration-selective neurons were first found in the midbrain torus semicircularis of anurans (4, 5), homolog of the mammalian inferior colliculus (IC) and referred to here as the IC_{an}. In anurans and many mammalian species, midbrain neurons have been identified that show short-pass, band-pass, or long-pass duration selectivity (3, 6–11). These neurons code for temporal properties of acoustic signals that are important in communication and echolocation. Processing sound duration is also critical for human speech communication, and deficiencies in the neural processing of this and other temporal information feature prominently in disorders of speech recognition (12, 13). Hence, understanding the mechanisms of duration selectivity is of considerable importance.

Several models of duration selectivity have been proposed. The first model, derived from extracellular recordings in the anuran IC (4), incorporates delayed, onset excitation and short-latency offset excitation that coincide for the optimal stimulus duration (Fig. 1*A*). Subsequent extracellular recordings from IC neurons in bats showed that blocking receptors of inhibitory neurotransmitters eliminated, or greatly attenuated, duration selectivity (14–16). Further, the temporal pattern of discharges shifted from offset to onset type following attenuation of inhibition. These results, along with the findings that first-spike latency did not increase directly with tone burst duration (17) and temporal masking experiments (18), suggested that sustained inhibition might be critical for generating duration tuning. Whole-cell patch recordings in bats (19, 20) provided direct evidence that interplay between excitation and inhibition contributed to duration selectivity. This work inspired a second type of coincidence model of duration selectivity (Fig. 1*B*) in which delayed, subthreshold excitation maximally summates with rebound from short-latency inhibition (and/or offset excitation) over a narrow range of durations. Alternatively, Fuzessery and Hall (21) proposed an anticoincidence model (Fig. 1*C*) in which inhibition tracks stimulus duration and overlaps temporally with delayed excitation only when tone burst duration exceeds a particular value; the phasic, delayed excitation is suprathreshold, and therefore, rebound from inhibition is not required. Subsequent whole-cell patch recordings from duration-selective neurons in the anuran IC provided some limited support for this latter model, at least for short-pass selectivity; short-latency inhibition appeared to track stimulus duration with little or no rebound depolarization at the offset of long-duration tone bursts (3, 22). The results of this earlier work, however, did not reveal critical properties of the excitatory input to short-pass neurons. First, the study did not address whether the amplitude of excitation changed with tone burst duration; if excitatory postsynaptic potential (EPSP) amplitude decreases with stimulus duration, short-pass selectivity could be a property of the inputs to IC neurons. Second, the former investigation did not determine whether the excitation was suprathreshold and phasic; both types of models require phasic excitation, which should be subthreshold in the case of the coincidence hypothesis. Further, this study did

Significance

Understanding how excitatory and inhibitory inputs are integrated to achieve sensory selectivity is an important, but elusive, goal in neuroscience. Whole-cell recordings in vivo have revealed excitation and inhibition, but the computational mechanisms are generally unclear. In the inferior colliculus, neurons exist that respond selectively to short-duration sounds; the mechanistic basis of this selectivity has long been debated. We combined whole-cell recordings, in vivo, with conductance extraction algorithms and focal pharmacological manipulations to show that duration selectivity results from an anticoincidence of suprathreshold excitation and inhibition. These results challenge the widely held view that postinhibitory rebound depolarization must coincide with subthreshold excitation to generate duration selectivity.

Author contributions: R.K.A., G.J.R., and C.J.L. designed research; R.K.A., G.J.R., J.L.H., C.J.L., G.A.V.-O., J.A.G., and J.W. performed research; R.K.A., G.J.R., C.J.L., and J.W. contributed new reagents/analytic tools; R.K.A., G.J.R., J.L.H., C.J.L., G.A.V.-O., and J.W. analyzed data; and R.K.A., G.J.R., J.L.H., C.J.L., and G.A.V.-O. wrote the paper.

The authors declare no conflict of interest.

This article is a PNAS Direct Submission.

[1]To whom correspondence should be addressed. Email: rose@bioscience.utah.edu.

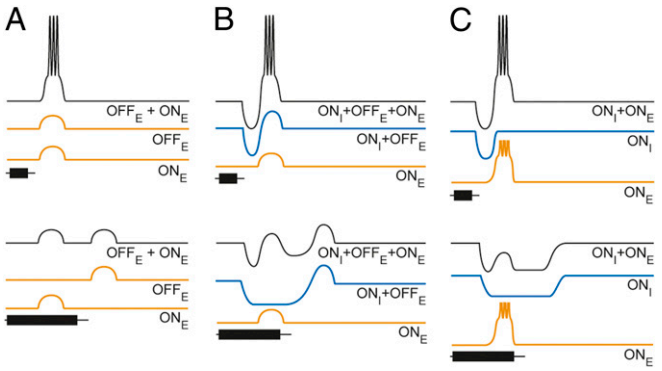

Fig. 1. Coincidence (*A* and *B*) and anticoincidence (*C*) models for duration selectivity (short-pass instantiation). (*B*) Adapted with permission from The American Physiological Society (refs. 14, 17); data from refs. 19, 20; and (*C*) data from ref. 21. Excitation (orange) is triggered by either stimulus onset (ON$_E$) or stimulus offset (OFF$_E$). Inhibition (blue) is triggered by stimulus onset (ON$_I$), with a shorter latency than that of ON$_E$. In *B*, the blue trace represents onset inhibition (ON$_I$) followed by postinhibitory rebound depolarization (OFF$_E$).

not test whether short-duration tone bursts elicit postinhibitory rebound depolarization.

To determine the mechanisms that underlie duration selectivity, we used mathematical models to estimate the time courses and magnitudes of excitatory and inhibitory conductances for IC$_{an}$ neurons across a range of tone burst durations. We also blocked GABA$_A$ or AMPA and NMDA receptors while making whole-cell recordings, in vivo, to evaluate the roles of stimulus-elicited inhibition and excitation in shaping duration selectivity. Using this constellation of methodologies, we show that selectivity for short-duration sounds arises from interplay between delayed phasic excitation, sustained inhibition that tracks stimulus duration, and active membrane properties. These results support an anticoincidence model of selectivity for short-duration sounds.

Results

Properties of Inhibition and Excitation to Short-Pass Neurons.

Inhibition tracks stimulus duration and counteracts delayed, phasic excitation. To investigate the integrative processes that underlie short-pass duration selectivity, we analyzed current clamp recordings (in vivo, whole-cell) from 26 short-pass neurons. We calculated changes in excitatory (Δg_e) and inhibitory (Δg_i) conductances using mathematical models (*Experimental Procedures*) for at least two stimulus durations in 16 of these cases; for three other neurons, we reconstructed conductance changes from responses to a single stimulus duration. These analyses provided estimates of the temporal dynamics of inhibition and excitation and enabled us to determine whether short-pass selectivity was already present in the inputs to IC$_{an}$ cells.

We first present recordings and profiles of Δg_i and Δg_e for three neurons that represent the range of short-pass duration selectivity that was observed (Fig. 2). The neuron shown in Fig. 3*A* represented those (~50%) that showed strong short-pass selectivity but responded weakly (≤1 spike/stimulus presentation). Tone bursts, ranging in duration from 10 to 160 ms, elicited primarily depolarizations, with spikes occurring only for the 10-ms stimuli (shortest duration tested). Depolarizations for 80 and 160 ms stimuli were more phasic than for shorter-duration tone bursts, particularly for recordings without negative current injected. Thus, although no early hyperpolarizations were observed, these findings suggested a role of inhibition in shaping response profiles. Conductance estimates confirmed that inhibition was present and revealed that the time courses of Δg_i and Δg_e were highly similar for 10-ms tone bursts (Fig. 3*A*, lower traces). This temporal congruence of conductance changes is consistent with the relatively small stimulus-elicited depolarizations and spike response of this cell. The duration of Δg_i increased approximately linearly with that of the stimulus, whereas Δg_e duration was relatively independent of tone burst duration. Across all cells (Fig. 3*B*), the Δg_i profiles in response to 40-, 80-, and 160-ms duration tone bursts were significantly longer than those for 20-ms tone bursts [Wilcoxon signed rank tests, $z = -2.36$, $P = 0.018$, $n = 7$ (20 vs. 40 ms); $z = -2.8$, $P = 0.005$, $n = 10$ (20 vs. 80 ms); $z = -2.98$, $P = 0.003$, $n = 12$ (20 vs. 160 ms)], whereas durations of Δg_e did not differ across these comparisons [Wilcoxon signed rank tests, $z = -1.86$, $P = 0.06$, $n = 7$ (20 vs. 40 ms); $z = -0.15$, $P = 0.88$, $n = 10$ (20 vs. 80 ms); $z = -0.53$, $P = 0.59$, $n = 12$ (20 vs. 160 ms)].

Results of conductance analyses across cells also indicated that excitatory inputs to these IC$_{an}$ neurons did not already show short-pass duration selectivity; peak amplitudes of excitatory conductances were highly similar for short and long tone burst durations [medians = 0.74 nS (20 ms) and 0.69 nS (160 ms); Wilcoxon signed rank test, $z = 1.26$, $P = 0.21$, $n = 12$]. Across short-pass cells, Δg_e peaks for responses to 20-ms tone bursts were ~29.9 ms delayed (median value, range = 2.2–56.7 ms) relative to those for Δg_i. Further, offsets of tone bursts did not trigger secondary peaks of excitation, as predicted from the coincidence model of Fig. 1*A*. These findings are consistent, therefore, with models of duration selectivity that incorporate short-latency, sustained inhibition and delayed, relatively phasic excitation (Fig. 1 *B* and *C*).

Active membrane properties amplify responses to short-duration sounds. The cell presented in Fig. 4*A* also showed strong short-pass selectivity (Fig. 2, open circles) but represents those (~19%) that responded strongly (≥2 spikes per repetition). For this neuron, short-duration tone bursts elicited a short-latency hyperpolarization followed by a longer-latency depolarization that reliably triggered spikes. As with the previous cell, the time courses of Δg_i tracked tone burst duration and almost entirely spanned those of Δg_e for 80- and 160-ms stimuli. Although peak Δg_e values were similar for all tone burst durations, the 80- and 160-ms stimuli elicited sustained hyperpolarizations, i.e., excitation, did not result in depolarization of the cell above its resting level. For 20-ms tone bursts, the time course of Δg_e exceeded that of Δg_i and resulted in delayed depolarization. Unlike in the previous case, however, depolarizations were largest for recordings that were made with little or no negative current injected, i.e., small levels of negative current clamp, suggesting that voltage-dependent processes also contributed to these EPSPs; the cells shown in Figs. 3*A* and 4*A* represent the two ends of the spectrum in this property.

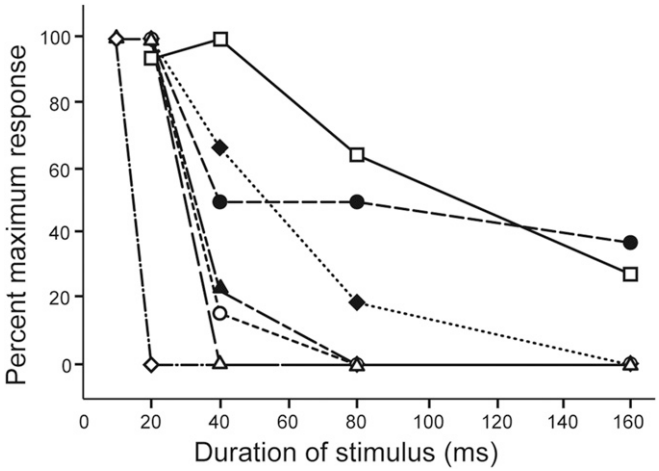

Fig. 2. Many midbrain neurons show selectivity for short-duration sounds. Normalized response (spikes/stimulus repetition) vs. tone burst duration for seven neurons that represented the observed range of short-pass duration selectivity.

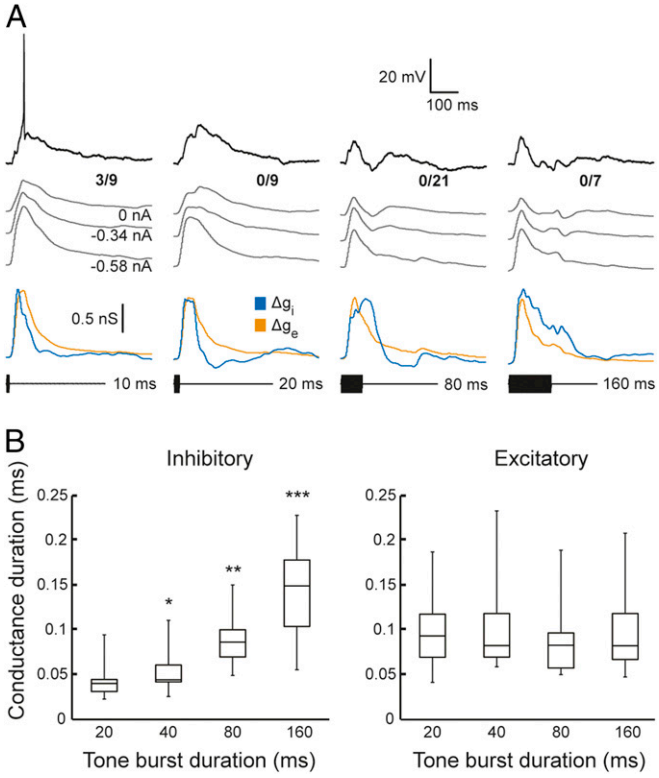

Fig. 3. The time course of inhibition, but not excitation, tracks stimulus duration. (*A*) Responses and conductance reconstructions for a short-pass duration-selective neuron that spiked only to 10-ms tone bursts. Representative membrane voltage responses for single presentations of tone bursts that had durations of 10, 20, 80, and 160 ms (black). Gray traces show averaged responses (spikes removed using median filter), used for estimating excitatory (orange) and inhibitory (blue) conductance changes; the amount of current injected for each current clamp level is shown at the tail for each averaged trace. The number of spikes elicited over the number of repetitions is shown at the right end of each response (0 nA current clamp). Resting potential = –98.0 mV; stimulus amplitude = 67 dB SPL; carrier frequency = 930 Hz (BEF of the neuron). (*B*) Duration of inhibitory and excitatory conductance changes versus tone burst duration for the population of short-pass neurons recorded. Conductance duration was measured as the time between points at 50% of maximum response on the initial–rising and final–falling phases of excitatory and inhibitory conductance change traces, such as those shown in *A*. Whiskers and boxes show the total range of values and interquartile ranges, respectively. Response sample sizes for the various stimulus durations are 20 ms (n = 14), 40 ms (n = 7), 80 ms (n = 10), and 160 ms (n = 12). Levels of significance for comparisons of conductance durations, relative to that for 20 ms, are denoted above boxes: *P < 0.05, **P < 0.01, and ***P < 0.005.

Across short-pass neurons, ∼52% of the variation in the strength of response (spikes/stimulus presentation) to short-duration tone bursts could be accounted for by the influence of active membrane properties on depolarizations (measured as the change in duration of depolarizations between recordings made across current clamp levels) ($F_{1,13}$ = 14.076, P = 0.002); depolarization duration (measured at 1/2 maximal amplitude) was relatively constant across current clamp levels for neurons that showed no evidence of active membrane properties (e.g., Fig. 3*A*).

Amplification of responses resulting from active membrane properties were evidenced as apparent negative (below baseline) changes in inhibitory conductance. These negative Δg_i phases were substantially reduced after recordings at 0-nA current clamp were excluded from the analyses (e.g., Fig. 4*A*, gray lines). Note that removing the recordings made without injected current from the analyses did not appear to alter the general time course of the positive phase of Δg_i (gray vs. blue lines) but contributed more noise to the trace.

Incomplete temporal overlap of excitation and inhibition for long-duration sounds is associated with broader duration tuning. The neuron shown in Fig. 4*B* (also depicted by open squares in Fig. 2) is representative of cells that showed broad-duration tuning (∼19%); unlike the former neurons, 160-ms tone bursts elicited spikes in this case. Analyses of recordings from this cell further illustrate how the time courses of Δg_i and Δg_e contribute to short-pass selectivity. As with most short-pass cells, a short-duration tone burst elicited an increase in excitatory conductance that reached its peak after that of the inhibitory conductance and had a longer time course (Fig. 4*B*); this temporal disjunction was associated with robust spiking. As was also seen with other short-pass cells, the time course of Δg_i for this neuron increased with tone burst duration. However, unlike the more selective short-pass cells, Δg_e for 80- and 160-ms tone bursts persisted beyond Δg_i and was associated with suprathreshold depolarizations following stimulus

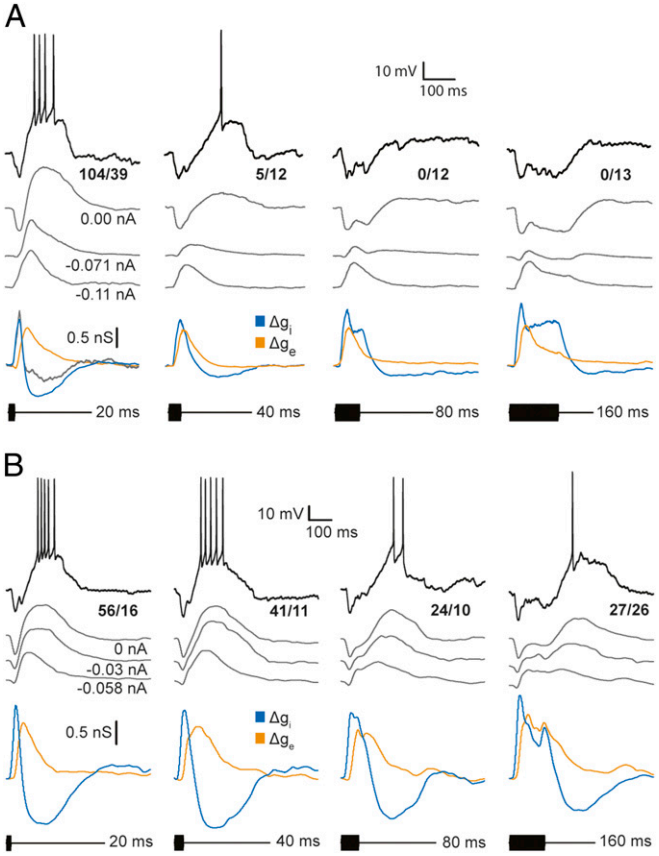

Fig. 4. Sharpness of duration tuning depends on the overlap of excitatory and inhibitory conductance changes in response to long-duration sounds. Whole-cell recordings and profiles of excitatory and inhibitory conductances for strongly selective (*A*) and weakly selective (*B*) short-pass neurons. Representative membrane potential responses to a single stimulus presentation (black) and averaged responses (gray traces) are shown; the number of spikes elicited over the number of stimulus repetitions is displayed for averaged responses (0 nA current clamp condition). Gray traces show averaged responses (spikes removed), recorded at the levels of current clamp indicated, used for reconstructing (estimating) the time courses of excitatory (orange) and inhibitory (blue) conductance changes. (*A*) The time course of inhibitory conductance for 20-ms tone bursts also was estimated using only the recordings at negative current clamp levels (gray trace). Resting potential = –65 mV; stimulus amplitude = 63 dB SPL; carrier frequency = 240 Hz (BEF of the neuron). (*B*) Resting potential = –74.5 mV; stimulus amplitude = 63 dB SPL; carrier frequency = 730 Hz (BEF of the neuron).

offset. This long-lasting excitation, coupled with sustained inhibition, appeared to underlie the increase in first-spike latency with tone burst duration and broad-duration tuning. As in the case shown in Fig. 4*A*, the depolarizations at stimulus offset were most prominent for recordings in which little or no negative current was injected.

Model estimates predict that excitation is suprathreshold. To assess whether excitation alone would be sufficient for triggering spikes, i.e., was suprathreshold, we used the estimated excitatory conductances from the cell shown in Fig. 3*A* in a single-compartment model (*Experimental Procedures*) to calculate the change in membrane potential that should occur in the absence of inhibition. For the Δg_e profile that was estimated from responses to 160-ms tone bursts, peak depolarizations of ~26 mV were calculated, which were at least 6 mV suprathreshold and substantially exceeded the 20-mV depolarization recorded for 10-ms tone bursts. In all cases, stimulus-driven Δg_e elicited depolarizations that were sufficiently large to activate voltage-dependent conductances, which promoted further depolarizations and spiking.

Attenuating Inhibition Broadens Duration Tuning by Unmasking Suprathreshold Excitation. Conductance estimates suggested that excitation was sufficiently strong to elicit spikes and relatively independent of tone burst duration; that is, Δg_e amplitude and duration were quite similar across tone burst durations. Short-pass selectivity appeared to result, therefore, because inhibition overlapped temporally and canceled excitation most effectively for long-duration stimuli. We predicted, therefore, that attenuating inhibition would unmask suprathreshold excitation for all stimulus durations. To test this hypothesis, we iontophoresed $GABA_A$ receptor antagonists (bicuculline or gabazine) to attenuate inhibition while making whole-cell recordings from seven short-pass neurons, in vivo; at least partial block was achieved in five of these cases. These challenging experiments represent the first instance to our knowledge of using this methodology to elucidate mechanisms of temporal selectivity in any system.

Whole-cell recordings from a short-pass neuron that were made before, during, and after iontophoresis of bicuculline are shown in Fig. 5. As with most (18/26) other short-pass cells, tone bursts elicited short-latency hyperpolarizations that tracked stimulus duration; depolarizations in response to 20-ms tone bursts occasionally triggered spikes. Following iontophoresis of bicuculline for ~2 min, depolarizations in response to 20-ms tone bursts increased in amplitude and reliably elicited spiking. Continued application of bicuculline further attenuated inhibition and decreased the short-pass selectivity of this neuron; 40-ms stimuli elicited maximum spike responses, and prominent suprathreshold depolarizations in response to 80- and 160-ms tone bursts were observed. After ~10 min of bicuculline iontophoresis, early hyperpolarizations were ~6.7 mV, versus 15 mV in baseline (pretreatment) recordings. The increased activity was associated with larger stimulus-elicited depolarizations, not a general decrease in the resting potential of the cell (note that the difference between the prestimulus membrane potential and the threshold for spike initiation was nearly constant throughout the experiment). Nearly full recovery of short-pass selectivity was observed ~5 min after terminating iontophoresis.

Inhibition was attenuated in three additional short-pass cells following iontophoresis of gabazine, a highly selective $GABA_A$ receptor antagonist; duration selectivity was decreased in all of these cells. Data from one of these cases are shown in Fig. 6. This neuron responded weakly to short-duration tone bursts but not to longer durations and showed no stimulus-induced hyperpolarizations; that is, it was similar to the cell shown in Fig. 3. As was typically seen for short-pass neurons, profiles of Δg_e were highly similar in time course and magnitude across stimulus durations, indicating that short-pass duration selectivity was not already present in the excitatory inputs to this cell. Although stimulus-driven

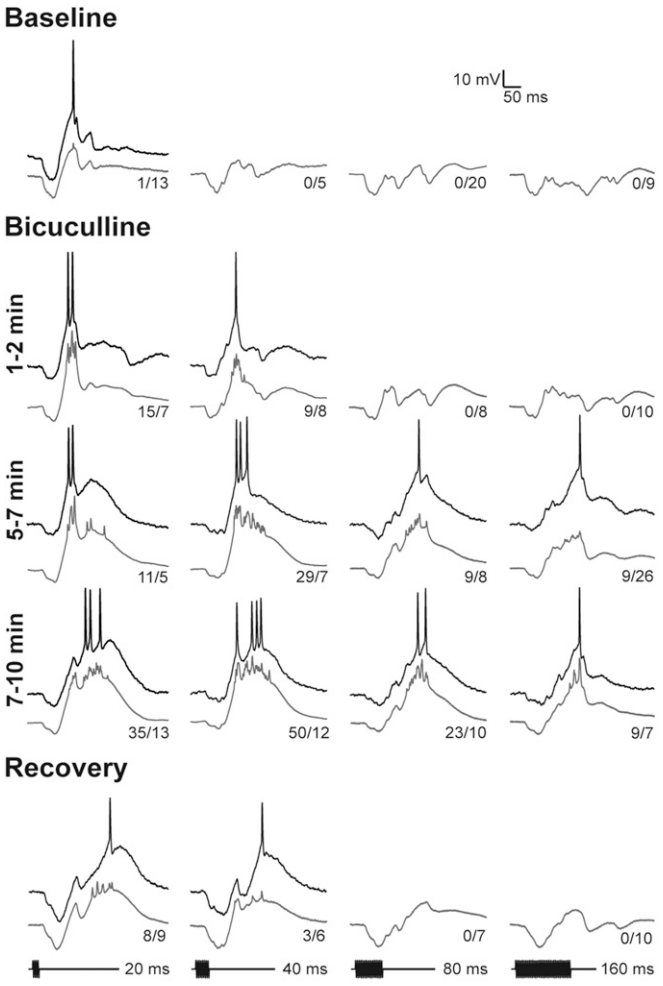

Fig. 5. Attenuating $GABA_A$ inhibition with bicuculline unmasks excitation to long-duration sounds and decreases short-pass duration selectivity. The $GABA_A$ receptor antagonist bicuculline (BIC) was iontophoresed (+70 nA); recordings were made at several times after starting iontophoresis and then ~5 min after stopping BIC (recovery). Single (black traces) and averaged (gray traces) responses are shown. The number of spikes elicited over the stimulus repetitions is shown at the tail of each averaged trace. Resting potential = −68 mV; stimulus amplitude = 71 dB SPL; carrier frequency = 200 Hz.

hyperpolarizations were not apparent in the recordings from this neuron, conductance estimates revealed that all stimulus durations elicited inhibition (Fig. 6). Short-pass selectivity appeared to result from an increase in the magnitude and time course of inhibition as tone burst duration was increased. Following 1–2 min of gabazine iontophoresis, the response to 20-ms tone bursts was increased, and 40-ms tone bursts elicited spikes. With continued gabazine delivery, depolarizations were further augmented, and all stimulus durations elicited spikes; again, first-spike latency was reduced, consistent with a role of inhibition in determining this response property. In this case, we were able to record at several levels of current clamp at this stage of gabazine iontophoresis. Analyses of these data revealed that Δg_i was attenuated for all tone burst durations, and Δg_e profiles were comparable to those measured before gabazine administration. Thus, attenuating inhibition unmasked excitation for all tone burst durations that were tested. In addition to increasing response strength, attenuating inhibition decreased the short-pass selectivity of this cell; after ~2.5 min of gabazine iontophoresis, response levels were similar for both 20- and 40-ms tone bursts. Nonetheless, some short-pass selectivity persisted (that is, response levels decreased at longer stimulus durations). This

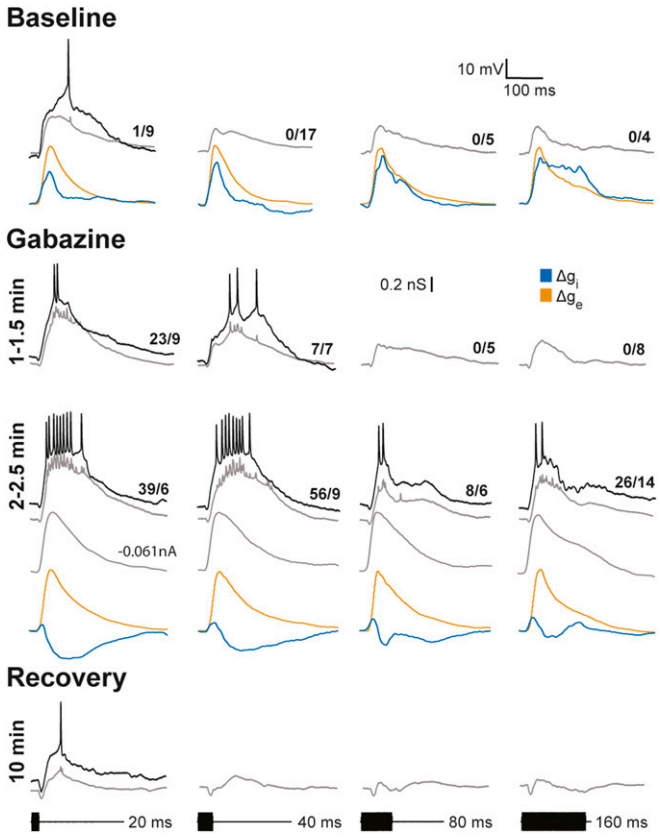

Fig. 6. Gabazine attenuates $GABA_A$ inhibition and decreases short-pass duration selectivity without decreasing excitation. Whole-cell recordings and reconstructions of inhibitory and excitatory conductances before and after focal iontophoresis (+70 nA) of gabazine (3 mM), a selective antagonist of $GABA_A$ receptors, to attenuate inhibition. Recordings were made at several times after starting iontophoresis and then ∼10 min after stopping iontophoresis (recovery). Single (black traces) and averaged (gray traces) responses recorded at 0.0 nA are shown; responses recorded at –0.061 nA of current clamp are also shown for the 2–2.5 min gabazine condition. The number of spikes elicited over the stimulus repetitions is shown at the tail of each averaged trace. Resting potential = –66 mV; stimulus amplitude = 44 dB SPL; carrier frequency = 650 Hz.

residual short-pass selectivity suggests that inhibition was attenuated but not eliminated. Further, at this stage of GABA receptor blockade, depolarizations in response to 20- and 40-ms stimuli were substantially greater in amplitude and duration than those to longer duration stimuli. These differences appeared to be due to voltage-dependent conductances, e.g., NMDA receptor-mediated activity, that augmented the amplitude and time course of depolarizations. In support of this conclusion, EPSP duration and amplitude were much more similar across stimulus durations in recordings made when the cell was hyperpolarized to near its inhibitory reversal potential (∼–92 mV) (Fig. 6, gray traces, –0.061 nA); these EPSPs mirrored the computed excitatory conductances across stimulus durations. Substantial recovery of response level, first-spike latency, and short-pass selectivity was observed ∼10 min after iontophoresis was terminated. At this stage of the recording, the resting potential of the neuron was ∼9 mV less negative, relative to that before and during the gabazine iontophoresis. Because of this depolarization, stimulus-elicited inhibition resulted in hyperpolarizations that increased with tone burst duration. Thus, gabazine reversibly attenuated inhibition and revealed suprathreshold excitation at all tone burst durations. These data further support the results of analyses of excitatory conductances; all tone burst durations that were tested elicited suprathreshold depolarizations. Short-pass selectivity did not result, therefore, from decreases in the strength of excitation as stimulus duration was increased; thus, short-pass selectivity in recorded cells does not appear to be a property inherited from afferent inputs.

Across cells, $GABA_A$ receptor antagonists increased the amplitude of stimulus-elicited depolarizations, particularly those for long-duration tone bursts (Fig. 7). Thus, attenuating inhibition unmasked the excitation that was present, thereby decreasing short-pass selectivity. Results of blocking $GABA_A$ receptors also fail to support coincidence-type models in which delayed excitation sums with postinhibitory rebound and/or offset excitation. These models predict that the amplitude of stimulus-elicited depolarizations should be reduced or similar in amplitude following block of inhibition; however, we found that the amplitude of these depolarizations increased.

Postinhibitory Rebound Is Not Observed Following Isolation of Inhibition. Results of the above experiments indicate that excitation in response to short- or long-duration tone bursts is suprathreshold, sometimes as a result of interplay with active membrane properties. Postinhibitory rebound depolarization is, therefore, not required for eliciting spikes in response to short-duration stimuli. The finding that many neurons were strongly short-pass selective despite showing little or no hyperpolarizations (e.g., Figs. 3 and 7) also supports this conclusion. Nevertheless we investigated whether postinhibitory rebound depolarization might contribute to responses. Rebound depolarization, a key feature of the coincidence model shown in Fig. 1*B*, was not observed following the offset of negative current injection or stimulus-elicited inhibition (Fig. 8*A*). In the latter experiments, we took advantage of the property that the frequency tuning of inhibition is generally broader than that of the excitation (23). We thus adjusted the frequency and amplitude of tone bursts to values that elicited primarily hyperpolarizations that were similar in amplitude to the inhibitory postsynaptic potentials (IPSPs) in response to best excitatory frequency (BEF) tone bursts of the same duration. The case displayed in Fig. 8*A* showed particularly prominent hyperpolarizations in response to 20- and 160-ms tone bursts at the BEF of the cell (black traces). However, little or no postinhibitory rebound depolarization was observed following tone bursts that elicited inhibition alone (Fig. 8*A*, blue traces). Across the six short-pass neurons that were

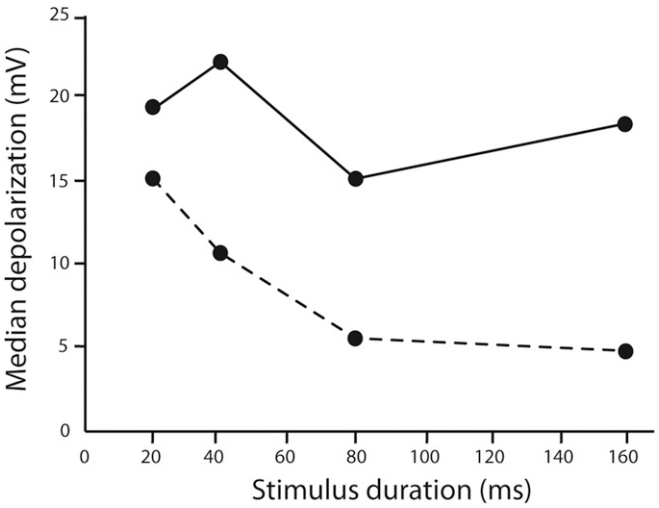

Fig. 7. Blocking inhibition increased stimulus-elicited depolarizations. Median amplitudes of depolarization responses of cells to tone bursts before (dashed line) and during (solid line) iontophoresis of $GABA_A$ receptor antagonists. Augmentation of depolarizations was greatest for responses to long-duration tone bursts.

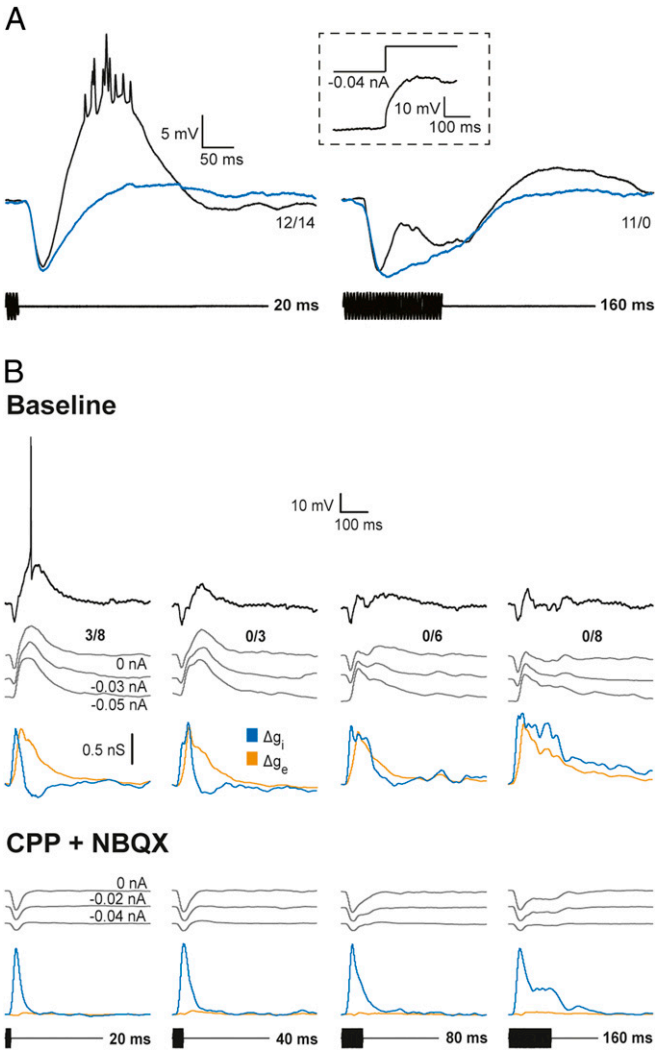

Fig. 8. Postinhibitory rebound was not observed. (*A*) Whole-cell recordings of responses to tone bursts of 190 Hz (black), the BEF of the neuron or 330 Hz (blue), which primarily elicited inhibition. (*Inset*) Response to release from −0.04-nA current injection. Resting potential = −82.2 mV; stimulus amplitude = 57 dB SPL. (*B*) Responses of a short-pass neuron before and after ∼8 min iontophoresis of NBQX (5 mM, +70 nA) and CPP (10 mM, +50 nA) to block AMPA- and NMDA-type glutamate receptors, respectively. Voltage recordings of responses to tone bursts (carrier frequency = 470 Hz) of various durations were made at the current clamp levels shown; estimates of changes in excitatory (orange) and inhibitory (blue) conductances are based on, and shown below, each set of these recordings. The number of spikes elicited over the number of repetitions is shown at the right end of each response (0-nA current clamp). Resting potential = −70.5 mV and −74 mV before and after blocking excitation, respectively; stimulus amplitude = 62 dB SPL.

tested in this manner, the mean postinhibitory rebound was 0.48 ± 0.36 mV (SE), and the mean stimulus-elicited hyperpolarization was 9.1 ± 1.36 mV. In contrast, the mean depolarization in response to short-duration tone bursts at the BEF of each cell was 13.6 ± 1.6 mV. These results suggest that postinhibitory rebound does not augment responses to short-duration tone bursts.

To further test for postinhibitory rebound, as postulated in the model shown in Fig. 1*B*, we pharmacologically isolated inhibition to short-pass neurons by iontophoresing 1,2,3,4-tetrahydro-6-nitro-2,3-dioxo-benzo [f]quinoxaline-7-sulfonamide disodium salt hydrate (NBQX) and 3-(2-carboxypiperazin-4-yl)-propyl-1-phosphonic acid (CPP) to block AMPA- and NMDA-type glutamate receptors, respectively. In the case shown in Fig. 8*B*, we also made whole-cell recordings at several levels of current clamp before and after attenuating excitation. This experiment also permitted the temporal structure of inhibition to be further characterized. Before iontophoresis of these antagonists, as was typical for short-pass neurons, this cell showed short-latency, positive Δg_i profiles that tracked tone burst duration and delayed Δg_e functions that had similar time courses across stimulus durations. Iontophoresis of NBQX and CPP strongly attenuated excitation to this cell; virtually no stimulus-driven depolarizations and increases in excitatory conductance were observed. Voltage recordings and Δg_i functions confirmed that inhibition had phasic onset and tonic components, and tracked tone burst duration. Further, postinhibitory rebound depolarizations, a key feature of the coincidence model shown in Fig. 1*B*, were not observed.

Before blocking glutamate receptors, voltage-dependent components of excitation could be seen as slightly augmented depolarizations for recordings with little or no negative current injected relative to those made at larger levels of negative current clamp, i.e., more hyperpolarized levels. These data indicate, therefore, that augmented depolarizations are primarily due to the action of excitation, not postinhibitory rebound. Removing excitation also enabled us to further identify the origin of apparent decreases in inhibitory conductances below baseline levels. Such decreases were not observed following block of excitation, consistent with the aforementioned postulate that they stem from voltage-dependent aspects of excitation, e.g., NMDA receptor-mediated excitation. The durations of the positive phase of Δg_i profiles at half-maximal amplitude were highly similar, however, for recordings before and after excitation was blocked, further showing that apparent decreases of inhibitory conductance below baseline did not appreciably influence these measurements of inhibitory time course. Thus, these pharmacological results strongly corroborated the findings from current clamp recordings (presented earlier).

Discussion

Our results strongly suggest that short-latency, sustained inhibition and delayed, phasic excitation are integrated to generate short-pass duration selectivity in the IC_{an}. In addition, for ∼68% of the cells, active membrane properties appeared to augment EPSP amplitude and enhance short-pass selectivity. Conductance estimates indicated that excitatory input to short-pass neurons was generally similar in amplitude and time course across tone burst durations, whereas inhibition tracked stimulus duration. Consistent with these findings, attenuating inhibition unmasked strong excitation in response to long-duration tone bursts and decreased short-pass selectivity. Blocking excitation to view inhibition in isolation confirmed that the inhibitory conductance shows a phasic increase at stimulus onset and a sustained component that tracks tone burst duration, particularly for responses to the 160-ms stimulus. Together, these results indicate, therefore, that short-pass selectivity emerges from integration of excitation and inhibition in the IC and is not generally present in the excitatory inputs to these cells. This is the first case to our knowledge of using this constellation of methodologies to elucidate the mechanisms that underlie selectivity for a temporal feature of sound.

Three general models of duration selectivity have been proposed. Following the initial discovery of duration-selective neurons in the anuran auditory midbrain, Narins and Capranica (4) proposed that duration selectivity could result from integration of delayed ON excitation and short-latency OFF excitation; for a particular stimulus duration, excitatory events triggered at stimulus onset and offset coincide in an AND-type operation to elicit spikes. OFF excitation could result from postinhibitory rebound in neurons that are presynaptic to temporal feature detecting cells, as has been observed in the auditory system of crickets (24). Our results support the delayed ON excitation component of this model, but OFF excitation does not appear to play an important role in short-pass duration selectivity.

Alternatively, whole-cell recordings from IC neurons in bats, and associated modeling studies, suggested that short-pass or band-pass selectivity might arise from coincidence of delayed, subthreshold excitation and rebound from tonic inhibition (2, 19) or offset excitation (25); if stimulus duration exceeds a particular value, inhibition overlaps and cancels excitation. Subsequent extracellular recordings in bats, however, showed that short-pass IC neurons responded strongly and duration selectivity was disrupted after bicuculline iontophoresis to block $GABA_A$ receptors (21). These authors proposed an anticoincidence model of short-pass duration selectivity in which phasic, suprathreshold excitation is integrated with shorter-latency, tonic inhibition; spikes occur as a result of anticoincidence of excitation and inhibition. However, because these were extracellular recordings, the possibility that bicuculline simply caused a decrease in the resting potential of neurons could not be ruled out. Our findings that excitation is phasic and delayed relative to inhibition, which shows a time course that tracks tone burst duration, are broadly consistent with both of these inhibition-based models. Results, however, more strongly support the anticoincidence model, at least for short-pass selectivity, because (*i*) excitatory conductance changes were sufficiently strong and broad in time course to generate suprathreshold depolarizations; (*ii*) after iontophoresing bicuculline or gabazine to attenuate inhibition, stimulus-elicited depolarizations were increased—without changes in resting potential—and neurons spiked to all tone burst durations, further showing that excitatory input to short-pass cells was suprathreshold; and (*iii*) after blocking excitation, little or no postinhibitory rebound depolarization was observed. The latter finding was somewhat surprising given some cases showed substantial depolarization at stimulus offset (e.g., Fig. 4). The resolution of this apparent paradox is that these depolarizations occurred when excitation extended beyond inhibition and was amplified by active membrane properties.

Active membrane properties primarily amplified depolarizations in response to short-duration stimuli and thereby contributed to short-pass selectivity. The effects of voltage-dependent conductances were particularly evident after attenuating inhibition and, in the case shown in Fig. 6, appeared to account, at least in part, for the observed residual duration tuning. Specifically, during the initial stage of GABA receptor blockade, EPSPs to short-duration (but not long-duration) tone bursts were sufficiently large for activating voltage-dependent conductances and elicited spikes. With increasing block of inhibition, excitation to longer-duration tone bursts was progressively unmasked and amplified by voltage-dependent conductances. We postulate that because inhibition was not blocked completely, short-pass selectivity was not eliminated; that is, long-duration stimuli failed to elicit depolarization sufficient for fully activating voltage-dependent conductances. An alternative hypothesis is that short-pass selectivity persisted after iontophoresis of GABA receptor antagonists because afferents were already duration selective. Negative current clamp recordings (i.e., driving force on inhibition was minimal) made during gabazine iontophoresis, however, revealed depolarizations that closely reflected the excitatory conductance profiles across tone burst durations and showed relatively little duration selectivity (Fig. 6); these results support the former hypothesis. Augmentation of excitation could result from activating voltage-dependent channels associated with NMDA-type receptors, which has been shown to contribute to rate-dependent enhancement of excitation in the mammalian IC (26). To test this hypothesis, NMDA receptors alone could be blocked while making whole-cell recordings from short-pass cells. Voltage-gated Na^+ channels might also contribute to amplification. In preliminary experiments, however, blocking voltage-gated Na^+ channels with intracellular delivery of QX-222 failed to attenuate this voltage-dependent augmentation.

The anticoincidence mechanism of duration selectivity may be functionally advantageous because of its inherent capacity for achieving level tolerance; as sound level increases, both inhibition and excitation should increase in strength, thereby maintaining short-pass selectivity (3). This interplay might enable animals to correctly identify conspecific calls over a wide range of amplitudes, such as those that female leopard frogs experience when approaching a calling male. Coincidence mechanisms, however, appear particularly suited for generating selectivity for midduration sounds, i.e., band-pass selectivity, as well as for pulse rate (24). Indeed, it appears that both coincidence and anticoincidence mechanisms can be used to generate selectivity for temporal features of sounds. The question thus arises whether the anticoincidence mechanism might be limited to short-pass duration selectivity. Within the anticoincidence framework, band-pass selectivity might result from decreasing the amplitude of excitatory conductances and using a higher proportion of NMDA-type receptors. Band-pass duration selectivity appears to be relatively rare in the anurans studied so far (3). Additional work is needed, therefore, to test this hypothesis.

We found that inhibition to duration short-pass neurons generally had a large, phasic onset component, followed by a weaker tonic component; this pattern was particularly evident in responses to the longer-duration stimuli. GABA receptor blockade attenuated both components of this stimulus-driven inhibition. It is presently unclear whether this residual inhibition resulted from incomplete block of GABA receptors or action of pharmacologically distinct inhibitory receptors. For example, iontophoresis of strychnine to block glycine receptors can attenuate inhibition in the IC of mammals, although to a lesser extent than after GABA receptor blockade (14). Also, glycine receptors on IC neurons may in some cases mediate paradoxical excitation (27). Further experiments are needed to test for a possible role of glycinergic inhibition in short-pass duration selectivity in the anuran IC.

Antagonists of GABA receptors, e.g., bicuculline and gabazine, have long been used in conjunction with extracellular recordings (28) to determine the role of inhibition in generating stimulus selectivity. Blockade of inhibition has been reported to decrease frequency tuning and selectivity for amplitude modulation rate (29–31) and duration (14, 19, 21). However, because generalized increases in activity also result from blocking GABA receptors, it is unclear whether stimulus-driven inhibition plays a direct role in determining selectivity (32). For example, bicuculline might simply reduce tonic inhibition and decrease the resting membrane potential of the cell, i.e., tonically depolarize the cell, thereby enabling suboptimal stimuli to elicit spikes. Also, bicuculline has been shown to attenuate Ca^{+2}-dependent K^+ conductances, which can result in depolarization and potentiation of NMDA-dependent burst firing (33). Such effects could account for conflicting evidence in studies of orientation selectivity in the visual system. Whole-cell patch recordings from visual cortical neurons showed, contrary to conclusions reached from pharmacologically blocking inhibition (34), that orientation selectivity can result from integration of excitatory thalamic inputs (35). Recent intracellular (particularly whole-cell) recordings have shown that biologically relevant stimuli can elicit diverse and complex patterns of excitation and inhibition in midbrain neurons (3, 19, 20, 23, 36–40), suggesting that inhibition plays important computational roles. Our results provide direct evidence that $GABA_A$ antagonists can attenuate stimulus-driven inhibition and markedly reduce short-pass duration selectivity; bicuculline and the more selective $GABA_A$ antagonist, gabazine, had similar effects. Further, these impairments of selectivity were independent of changes in resting potential, and decreased selectivity was observed even though response saturation was not present (e.g., before GABA receptor antagonists had their full effect) (Figs. 5 and 6) or in recordings made with negative current clamp (Fig. 6). The finding that GABA receptor blockade unmasked prominent excitation in response to previously ineffective

stimuli, e.g., 160-ms tone bursts, demonstrates that stimulus-specific inhibition plays important roles in duration selectivity and that $GABA_A$ antagonists can attenuate this stimulus-driven inhibition. Additional studies that combine whole-cell recording and pharmacological manipulations are required to further test the generality of this result and the utility of this methodology.

Experimental Procedures

Surgical Preparation. All animal studies were conducted in compliance with the National Institutes of Health guidelines and were approved by The University of Utah's Institutional Animal Care and Use Committee. Wild-caught male and female northern leopard frogs (*Lithobates pipiens*) were prepared for neurophysiological experiments according to previously described methods (41). Frogs were anesthetized by immersion in 3% (wt/vol) urethane or 0.1% MS-222 and by topical application of 2% (wt/vol) lidocaine hydrochloride to the skin of the dorsal surface of the head, where a small craniotomy was performed to expose the optic tectum. After an overnight recovery period, frogs were immobilized by intramuscular injection of pancuronium bromide (4 μg/g) for electrophysiological recordings. Whole-cell patch recordings were made from 58 duration-selective neurons in the IC_{an}, in vivo, according to methods described previously (23, 42); 26 of these were short-pass cells. Recordings were made in an audiometric chamber that was maintained at 18–20 °C.

Electrode Construction. Patch pipettes were constructed from high-borate borosilicate capillary glass [Schott #8250, A-M Systems #5960; 1-mm outer diameter (OD), 0.58-mm inner diameter (ID)] using a Flaming/Brown type puller (model P-97; Sutter Instruments). These pipettes had outside tip diameters of ∼1.1–1.3 μm. Electrode tips were back-filled with a solution (pH = 7.4) consisting of (values in mM) 100 potassium gluconate, 2 KCl, 1 $MgCl_2$, 5 EGTA, 10 Hepes, 20 KOH, and 20 biocytin. Biocytin was replaced by mannitol (20 mM) in the solution used to fill pipette shanks. These pipettes had resistances between 10 and 25 MΩ. Extracellular recording pipettes were manufactured from the same glass used for making patch pipettes but had tip diameters of 2–3 μm and were filled with 2 M NaCl; resistances varied between 0.7 and 1.0 MΩ.

Whole-Cell Recording Procedure. Whole-cell recordings were made with patch-type pipettes, as described previously (42). Briefly, recording pipettes were advanced into the brain using an inchworm microdrive (model 6000 Controller; Burleigh Corp.) or a three-axis microdrive (model IVM-3000; Scientifica PLC) while applying positive pressure to the pipette fluid. After reaching the location for whole-cell recording, the pipette was advanced in 1.5-μm increments while maintaining positive pressure and passing −0.1-nA square-wave pulses (500 ms) to monitor resistance; cell contact was indicated by a small increase (10%) in the voltage change. Negative pressure was then applied to the pipette to increase the seal resistance to gigaohm levels. Subsequent to seal formation, negative current (∼−0.5 nA) was applied to rupture the patch and attain a whole-cell recording. Seal resistances were typically greater than 1.5 GΩ. Reported resting potentials are uncorrected for liquid junction potential.

Pharmacological Procedure. Drugs were delivered by iontophoresis, using three- to five-barrel micropipettes, which were manufactured from multibarrel, with microfilament, borosilicate capillary glass (Corning #7740, A-M Systems; 1.2-mm OD, 0.60-mm ID) using a vertical puller (model PE-2; Narishige). The tips of multibarrel pipettes were visualized under a stereo-dissecting microscope and broken to 10–15 μm diameter. Individual barrels were filled with L-glutamate (100 mM, pH = 8.0), NaCl (150 mM) for current balance, 20 mM bicuculline methiodide (in 150 mM NaCl, pH = 3.0), gabazine (3 mM in 150 mM NaCl, pH = 4.0) to block $GABA_A$ receptors, and 5 mM NBQX (pH 9.0 in 150 mM NaCl) or 10 mM CPP (pH = 8.0 in 150 mM NaCl) to block AMPA/Kainate or NMDA-type glutamate receptors, respectively. Each barrel of the assembly was connected via an Ag/AgCl wire to a constant-current iontophoresis device (model 6400; Dagan Corp.); to minimize recording noise, the power supply was located peripheral to the instrument. Approximately 50–100 nA constant current was used to iontophoretically deliver pharmacological compounds (negative for glutamate, NBQX, and CPP and positive for other agents). As described previously (43), two electrodes were concurrently used in these experiments. We iontophoresed glutamate to activate recorded cells, thereby evaluating whether the multibarrel pipette was sufficiently close to the recording pipette for conducting pharmacological manipulations. To minimize leakage of agents, retention currents of ∼5 nA (opposite the polarity used to deliver the agents) were applied to barrels that contained drugs. Multibarrel pipettes were advanced into the brain using a single-axis hydraulic manipulator (model MX610; Siskiyou Corporation).

Stimulus Generation and Delivery. Acoustic stimuli were generated using an auditory stimulus generator (systems II and III; Tucker Davis Technologies) and custom software developed in MATLAB environment (MathWorks, Inc.). Search stimulus carrier frequencies were systematically varied from 150 to 1,600 Hz with modulation frequencies (in the case of sinusoidal amplitude modulation) ranging from 10 to 100 Hz. Tone burst stimuli had rise/fall times of 1 ms. Stimuli were presented free-field in an audiometric room (41).

Data Acquisition and Analyses. Recordings were acquired and digitized at 10 kHz using a data acquisition interface (Model: Power 1401; Cambridge Electronic Design), then stored and analyzed using Spike2 software, also from the same supplier.

The time courses of excitatory and inhibitory conductances were estimated from whole-cell recordings at several levels of current clamp, using a least-squares adaptation (described below) of the algorithm outlined by Priebe and Ferster (44). This method was selected over voltage clamp techniques because of errors from incomplete space clamp associated with the latter when applied to central neurons (45, 46). Also, recordings at various levels of current clamp provided information relevant to understanding mechanisms of duration selectivity. When present, spikes were removed from recordings using a median filter. The passive response properties of a neuron were approximated using a single-compartment model, represented by the following first-order differential equation:

$$C_m\, dV_m/dt = -[\Delta g_i(V_m - E_i) + \Delta g_e(V_m - E_e) + g_{leak}(V_m - E_{rest})] + I_{inj},$$

where C_m is the cell capacitance, E_i and E_e are the reversal potentials of the inhibitory and excitatory conductances, V_m is the membrane potential, $g_{leak} = 1/R_{input}$ (represents the sum of conductances responsible for holding the cell at its resting potential, E_{rest}), and I_{inj} is the current injected into the cell through the patch pipette (electrode). The input resistance (R_{input}) and time constant (τ) were estimated from brief negative current pulses delivered to the neuron; the voltage drop across the electrode and access resistances, which had a fast time course, was subtracted from the total voltage change produced by these current injection steps. The mean input resistance of neurons in this study was ∼766 MΩ, SD = 360 MΩ. The capacitance of each neuron was calculated as $C = \tau/R_{input}$. The changes in excitatory conductance (Δg_e) and inhibitory conductance (Δg_i) resulting from stimulus presentation were the two unknowns to be estimated.

We used a least squares method (47) to estimate the unknown parameters (Δg_e and Δg_i). This minimization process involved overdetermining the system, i.e., using recordings at multiple levels of negative current clamp (injected current) to obtain more equations than the number of unknown parameters. We approximated Δg_e and Δg_i at each sample point in time (0.1 ms) as the values that provided the best fit, i.e., minimized the difference between measured and calculated changes in membrane potential, for the recordings across all current clamp levels. Conductance duration was measured as the time between points at 50% of maximum response on the initial–rising and final–falling phases of conductance traces.

Errors in measured values of membrane potential at various levels of negative current clamp can result from the voltage drop across the electrode and access resistances. In addition to measuring this voltage drop and subtracting it from the apparent membrane potential, we used a spike threshold-based method of determining V_m (48). This approach is based on the assumption that spike threshold for a particular neuron should, on average, be constant across current clamp conditions. Thus, to determine the actual membrane potential following current injection, the spike threshold drop was subtracted from the apparent membrane potential change.

The inhibitory reversal potential for each cell was estimated to be the V_m at which IPSPs reversed from hyperpolarizations to depolarizations; in some cases, carrier frequencies that elicited primarily inhibition were used for determining these reversal potentials. The excitatory reversal potential was generally taken to be approximately −20 to −40 mV, based on measurements where EPSPs were reversed from depolarizations to hyperpolarizations. Although the relative magnitudes of Δg_e and Δg_i changed slightly for different values of these reversal potentials, the time courses of these conductances were not affected. The computed Δg_e and Δg_i values represent estimates of stimulus-related changes in conductances relative to prestimulus baseline levels; background (no stimulus present) excitatory and inhibitory conductances contributed to the leak conductance, g_{leak}. Recordings without current injection and at small levels of current clamp in some cases

showed evidence of active membrane properties that amplified depolarizations. Including these recordings in analyses did not alter the time courses of the positive phase of Δg_i; however, these active properties were evidenced as apparent decreases in Δg_i below baseline. Negative Δg_i values could be minimized or eliminated by excluding such recordings from the analyses; however, the resulting conductance traces showed lower signal-to-noise ratios. A trade-off exists, therefore, between including vs. excluding recordings with active conductances. Because the time course of the positive phases of Δg_i and Δg_e did not differ between these two conditions, recordings at small levels of current clamp were generally included in the conductance analyses, thereby obtaining reconstructions that had greater signal-to-noise ratios.

ACKNOWLEDGMENTS. We thank Caleb Herrick and Harsha Gadhiraju for technical assistance. This work was supported by the National Institute on Deafness and other Communication Disorders Grant R01 DC0003788.

1. Aubie B, Sayegh R, Faure PA (2012) Duration tuning across vertebrates. *J Neurosci* 32(18):6373–6390.
2. Sayegh R, Aubie B, Faure PA (2011) Duration tuning in the auditory midbrain of echolocating and non-echolocating vertebrates. *J Comp Physiol A Neuroethol Sens Neural Behav Physiol* 197(5):571–583.
3. Leary CJ, Edwards CJ, Rose GJ (2008) Midbrain auditory neurons integrate excitation and inhibition to generate duration selectivity: An in vivo whole-cell patch study in anurans. *J Neurosci* 28(21):5481–5493.
4. Narins PM, Capranica RR (1980) Neural adaptations for processing the two-note call of the Puerto Rican treefrog, Eleutherodactylus coqui. *Brain Behav Evol* 17(1):48–66.
5. Potter HD (1965) Mesencephalic auditory region of the bullfrog. *J Neurophysiol* 28(6): 1132–1154.
6. Brand A, Urban R, Grothe B (2000) Duration tuning in the mouse auditory midbrain. *J Neurophysiol* 84(4):1790–1799.
7. Chen G-D (1998) Effects of stimulus duration on responses of neurons in the chinchilla inferior colliculus. *Hear Res* 122(1-2):142–150.
8. Pérez-González D, Malmierca MS, Moore JM, Hernández O, Covey E (2006) Duration selective neurons in the inferior colliculus of the rat: Topographic distribution and relation of duration sensitivity to other response properties. *J Neurophysiol* 95(2): 823–836.
9. Pinheiro AD, Wu M, Jen PH-S (1991) Encoding repetition rate and duration in the inferior colliculus of the big brown bat, Eptesicus fuscus. *J Comp Physiol A Neuroethol Sens Neural Behav Physiol* 169(1):69–85.
10. Wang J, van Wijhe R, Chen Z, Yin S (2006) Is duration tuning a transient process in the inferior colliculus of guinea pigs? *Brain Res* 1114(1):63–74.
11. Macías S, Mora EC, Hechavarría JC, Kössl M (2011) Duration tuning in the inferior colliculus of the mustached bat. *J Neurophysiol* 106(6):3119–3128.
12. Amenedo E, Escera C (2000) The accuracy of sound duration representation in the human brain determines the accuracy of behavioural perception. *Eur J Neurosci* 12(7): 2570–2574.
13. Nenonen S, Shestakova A, Huotilainen M, Näätänen R (2003) Linguistic relevance of duration within the native language determines the accuracy of speech-sound duration processing. *Brain Res Cogn Brain Res* 16(3):492–495.
14. Casseday JH, Ehrlich D, Covey E (2000) Neural measurement of sound duration: Control by excitatory-inhibitory interactions in the inferior colliculus. *J Neurophysiol* 84(3):1475–1487.
15. Fuzessery ZM, Razak KA, Williams AJ (2011) Multiple mechanisms shape selectivity for FM sweep rate and direction in the pallid bat inferior colliculus and auditory cortex. *J Comp Physiol A Neuroethol Sens Neural Behav Physiol* 197(5):615–623.
16. Wu C-H, Jen PH-S (2006) The role of GABAergic inhibition in shaping duration selectivity of bat inferior collicular neurons determined with temporally patterned sound trains. *Hear Res* 215(1-2):56–66.
17. Ehrlich D, Casseday JH, Covey E (1997) Neural tuning to sound duration in the inferior colliculus of the big brown bat, Eptesicus fuscus. *J Neurophysiol* 77(5):2360–2372.
18. Faure PA, Fremouw T, Casseday JH, Covey E (2003) Temporal masking reveals properties of sound-evoked inhibition in duration-tuned neurons of the inferior colliculus. *J Neurosci* 23(7):3052–3065.
19. Casseday JH, Ehrlich D, Covey E (1994) Neural tuning for sound duration: role of inhibitory mechanisms in the inferior colliculus. *Science* 264(5160):847–850.
20. Covey E, Kauer JA, Casseday JH (1996) Whole-cell patch-clamp recording reveals subthreshold sound-evoked postsynaptic currents in the inferior colliculus of awake bats. *J Neurosci* 16(9):3009–3018.
21. Fuzessery ZM, Hall JC (1999) Sound duration selectivity in the pallid bat inferior colliculus. *Hear Res* 137(1-2):137–154.
22. Rose GJ (2014) Time computations in anuran auditory systems. *Front Physiol* 5:206.
23. Edwards CJ, Leary CJ, Rose GJ (2007) Counting on inhibition and rate-dependent excitation in the auditory system. *J Neurosci* 27(49):13384–13392.
24. Schöneich S, Kostarakos K, Hedwig B (2015) An auditory feature detection circuit for sound pattern recognition. *Sci Adv* 1(8):e1500325.
25. Aubie B, Becker S, Faure PA (2009) Computational models of millisecond level duration tuning in neural circuits. *J Neurosci* 29(29):9255–9270.
26. Wu SH, Ma CL, Kelly JB (2004) Contribution of AMPA, NMDA, and GABA(A) receptors to temporal pattern of postsynaptic responses in the inferior colliculus of the rat. *J Neurosci* 24(19):4625–4634.
27. Sanchez JT, Gans D, Wenstrup JJ (2008) Glycinergic "inhibition" mediates selective excitatory responses to combinations of sounds. *J Neurosci* 28(1):80–90.
28. Havey DC, Caspary DM (1980) A simple technique for constructing 'piggy-back' multibarrel microelectrodes. *Electroencephalogr Clin Neurophysiol* 48(2):249–251.
29. Grothe B (1994) Interaction of excitation and inhibition in processing of pure tone and amplitude-modulated stimuli in the medial superior olive of the mustached bat. *J Neurophysiol* 71(2):706–721.
30. Lu Y, Jen PH-S, Wu M (1998) GABAergic disinhibition affects responses of bat inferior collicular neurons to temporally patterned sound pulses. *J Neurophysiol* 79(5): 2303–2315.
31. Yang L, Pollak GD (1997) Differential response properties to amplitude modulated signals in the dorsal nucleus of the lateral lemniscus of the mustache bat and the roles of GABAergic inhibition. *J Neurophysiol* 77(1):324–340.
32. Caspary DM, Palombi PS, Hughes LF (2002) GABAergic inputs shape responses to amplitude modulated stimuli in the inferior colliculus. *Hear Res* 168(1-2):163–173.
33. Johnson SW, Seutin V (1997) Bicuculline methiodide potentiates NMDA-dependent burst firing in rat dopamine neurons by blocking apamin-sensitive Ca2+-activated K+ currents. *Neurosci Lett* 231(1):13–16.
34. Sillito AM, Kemp JA, Milson JA, Berardi N (1980) A re-evaluation of the mechanisms underlying simple cell orientation selectivity. *Brain Res* 194(2):517–520.
35. Ferster D, Chung S, Wheat H (1996) Orientation selectivity of thalamic input to simple cells of cat visual cortex. *Nature* 380(6571):249–252.
36. Baker CA, Carlson BA (2014) Short-term depression, temporal summation, and onset inhibition shape interval tuning in midbrain neurons. *J Neurosci* 34(43):14272–14287.
37. Carlson BA (2009) Temporal-pattern recognition by single neurons in a sensory pathway devoted to social communication behavior. *J Neurosci* 29(30):9417–9428.
38. Edwards CJ, Leary CJ, Rose GJ (2008) Mechanisms of long-interval selectivity in midbrain auditory neurons: Roles of excitation, inhibition, and plasticity. *J Neurophysiol* 100(6):3407–3416.
39. Gittelman JX, Li N, Pollak GD (2009) Mechanisms underlying directional selectivity for frequency-modulated sweeps in the inferior colliculus revealed by in vivo whole-cell recordings. *J Neurosci* 29(41):13030–13041.
40. Kuo RI, Wu GK (2012) The generation of direction selectivity in the auditory system. *Neuron* 73(5):1016–1027.
41. Alder TB, Rose GJ (2000) Integration and recovery processes contribute to the temporal selectivity of neurons in the midbrain of the northern leopard frog, *Rana pipiens*. *J Comp Physiol A Neuroethol Sens Neural Behav Physiol* 186(10):923–937.
42. Rose GJ, Fortune ES (1996) New techniques for making whole-cell recordings from CNS neurons in vivo. *Neurosci Res* 26(1):89–94.
43. Rose GJ, et al. (2013) Combining pharmacology and whole-cell patch recording from CNS neurons, in vivo. *J Neurosci Methods* 213(1):99–104.
44. Priebe NJ, Ferster D (2005) Direction selectivity of excitation and inhibition in simple cells of the cat primary visual cortex. *Neuron* 45(1):133–145.
45. Williams SR, Mitchell SJ (2008) Direct measurement of somatic voltage clamp errors in central neurons. *Nat Neurosci* 11(7):790–798.
46. Bar-Yehuda D, Korngreen A (2008) Space-clamp problems when voltage clamping neurons expressing voltage-gated conductances. *J Neurophysiol* 99(3):1127–1136.
47. Harter H (1983) Least squares. *Encyclopedia of Statistical Sciences* (Wiley, New York), pp 340–351.
48. Anderson JS, Lampl I, Gillespie DC, Ferster D (2001) Membrane potential and conductance changes underlying length tuning of cells in cat primary visual cortex. *J Neurosci* 21(6):2104–2112.